CHAPTER VI

Optical and electrical properties of core-shell nanostructured films

In the earlier chapters, we have discussed in details about various core-shell nanostructures. We found that those core-shell nanostructures favour charge separation more than the core counterpart resulting in far better photocatalytic activity than the latter. Again TiO_2 based photovoltaic devices have been termed as centers of attraction since decades. TiO_2 and its corresponding core-shell nanostructures are most probably the highest used material in DSSCs. For any material to be used as a photovoltaic device, the prime factors which influences are: charge generation, charge separation and charge transport. The core-shell nanoparticles exhibited fabulous charge separation as we mentioned earlier. So, we aimed to work on core-shell films with these two questions:

- What are novelties that unfold if we optically and electrically characterize core-shell films?
- Can these films be used as photoanode in a photovoltaic device which is fabricated with a very simple and cost effective laboratory method?

To find answers to these queries, we first prepared the core-shell films with a standard procedure. Then the optical study was performed with the help of UV-vis absorbance spectra and PL spectra. We also characterized the films through XRD to assure the structural properties. Then we opted for electrical characterization followed by fabrication of a very simple photovoltaic device.

6.1   Preparation of TiO_2 film

The TiO_2 paste was prepared by grinding with a pestle by taking 6 g of TiO_2 nanopowder (Prepared by as described in chapter 2) and 2.4 g of polyethylene glycol (PEG 20000) (Merck, reagent grade) in 2 mL of distilled H_2O and 0.2 mL of acetylacetone (Aldrich, reagent grade) in a mortar for 40 min. Finally, 8.0 mL of distilled water and 0.1 mL of Triton X-100 (Aldrich, reagent grade) were slowly added under continuous mixing for 10 min [1]. Several drops of this suspension were spread onto the electrode surface (ITO coated glass) using a glass rod. The electrode was dried in air and heated at $450^{°}$C for 30 min.

6.1.1 Core-shell films

We prepared TiO_2-MgO, TiO_2-SnO_2 and TiO_2-ZrO_2 films by coating the as synthesized TiO_2 film with $Mg(OH)_2$, SnO_2 and ZrO_2 solution respectively as we prepared in the earlier chapters.
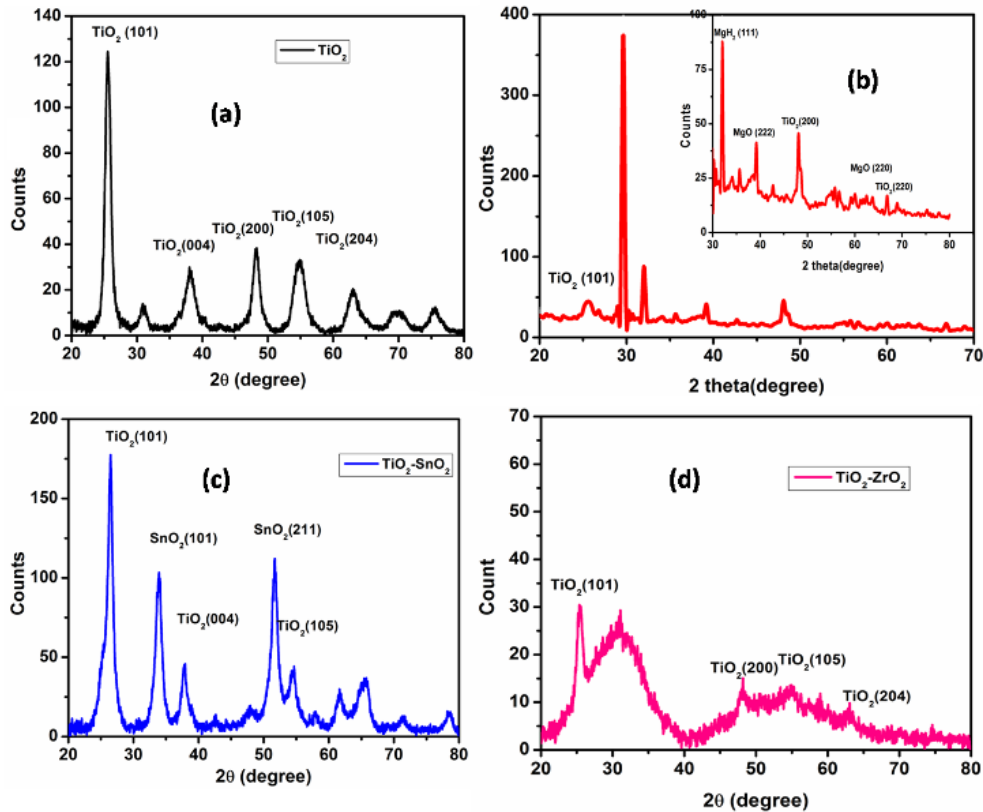
6.1.1.1 XRD pattern analysis

Fig 6.1: XRD pattern of (a) TiO_2 (b) TiO_2-MgO (c) TiO_2-SnO_2 and (d) TiO_2-ZrO_2 films

Fig 6.1 depicts the XRD pattern of all the core-shell films along with core TiO_2 film. From the curves, we can see that core-shell TiO_2-MgO and TiO_2-SnO_2 films contain phases of both core and shell. But in case of TiO_2-ZrO_2 core-shell film, no additional peak of ZrO_2 is found only the TiO_2 related peaks are broadened as well as shifted towards higher angles. This confirms presence of an additional material which is incorporated to TiO_2. Thus from the XRD pattern, the structural compositions of the films are cleared.

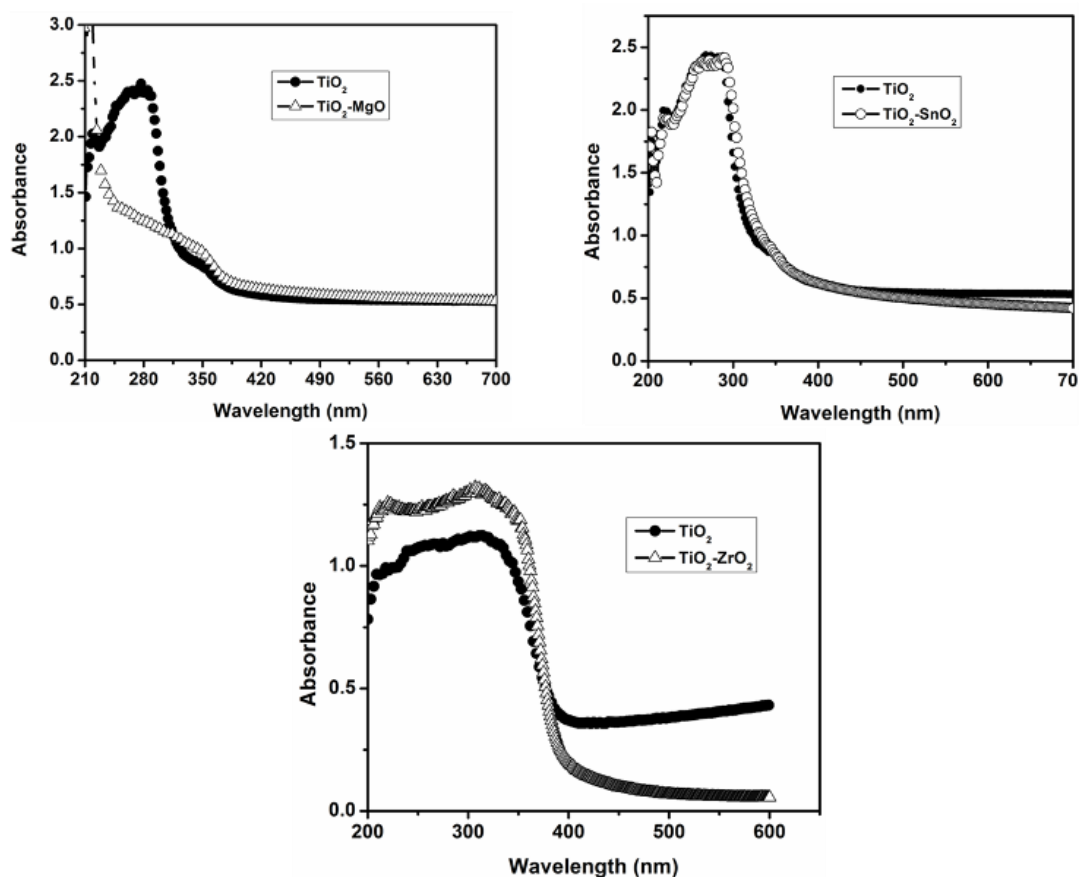### 6.1.1.2 UV-vis absorbance spectra analysis

Fig. 6.2: UV-vis absorbance spectra of the films

As we can see in Fig. 6.2, the TiO_2 film shows sharp UV absorbance. The absorption tail in the visible region occurs owing to the presence of Ti^{3+} or oxygen vacancies [2-4]. Generally, in TiO_2 nanoparticles, Ti^{4+} is surrounded by six oxygen ions forming basic TiO_6^{2-} octahedra. Loss of oxygen in the lattice allows the free electrons to get realesed. These free electrons are either captured by Ti^{4+} to form Ti^{3+} on the lattice site, to preserve charge neutrality, or got trapped in the oxygen vacancies. The electrons captured by the Ti^{4+}, on either side of oxygen vacancy (V_o), forms Ti^{3+}-V_o-Ti^{3+} defect complex yielding color centers (F, F^+ or F^{++}) [3-4]. Aside from colour centers, Ti^{3+} also exhibits absorptions between 2.2-2.3 eV (539-563 nm) due to $2T_2$ to $2E$ d-d transition of $d1Ti^{3+}$ [2].

In core-shell TiO_2-MgO and TiO_2-SnO_2 films, it can be clearly seen that the core-shell films also exhibit visible region absorbance like the core counterpart. But an anomaly

has occurred in core-shell TiO_2-ZrO_2 film as the visible regime absorbance has reached almost zero level. This may be due to quenching of defect related states in the sample.
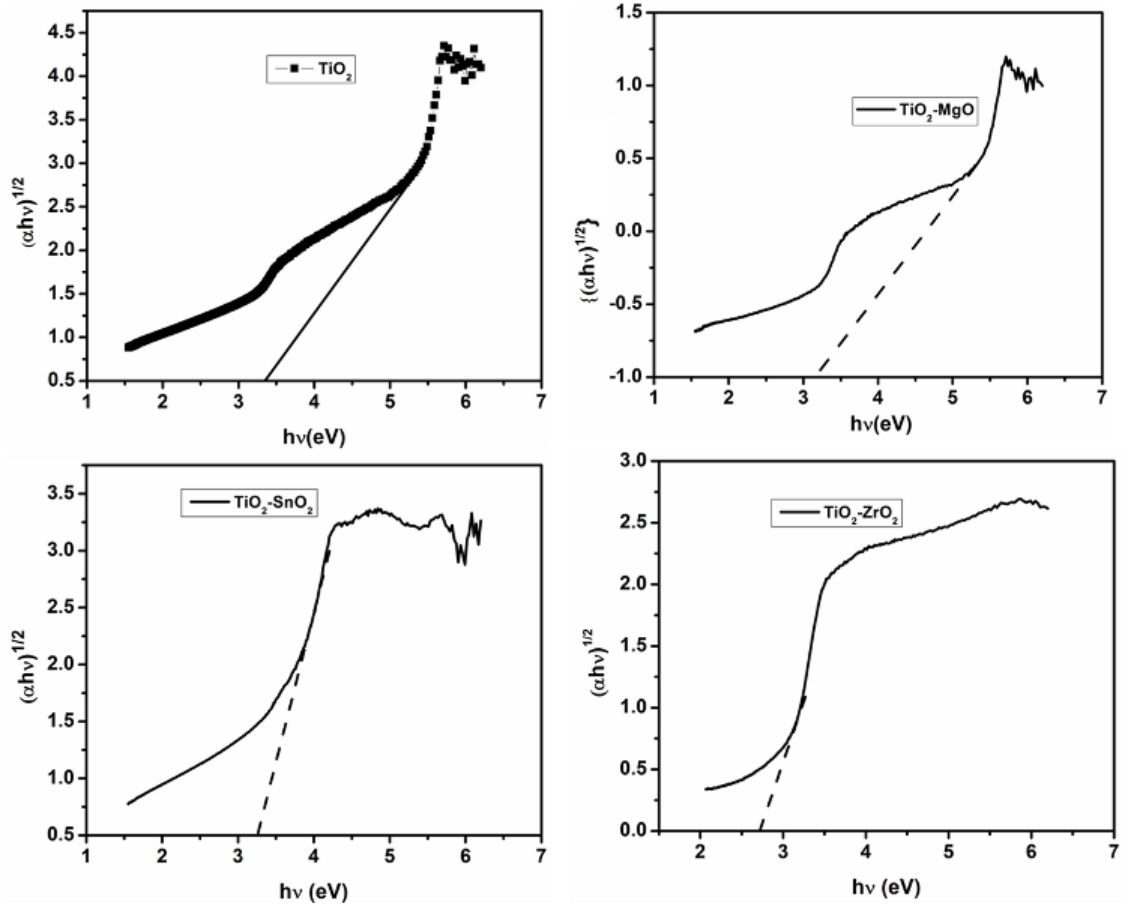

Fig. 6.3: Band gap determination from Tauc's Plot

The absorption coefficient, α, due to interband transition near the band-gap is well described by

$$\alpha\hbar\omega = B\,(\hbar\,\omega - E_g)^n \ldots\ldots\ldots\ldots(6.1).$$

where $n=1/2$ for indirect band gap semiconductor and 2 for direct band gap. $\hbar\omega$ is photon energy, E_g is optical gap. This Tauc plot defines the optical gap in amorphous semiconductors.
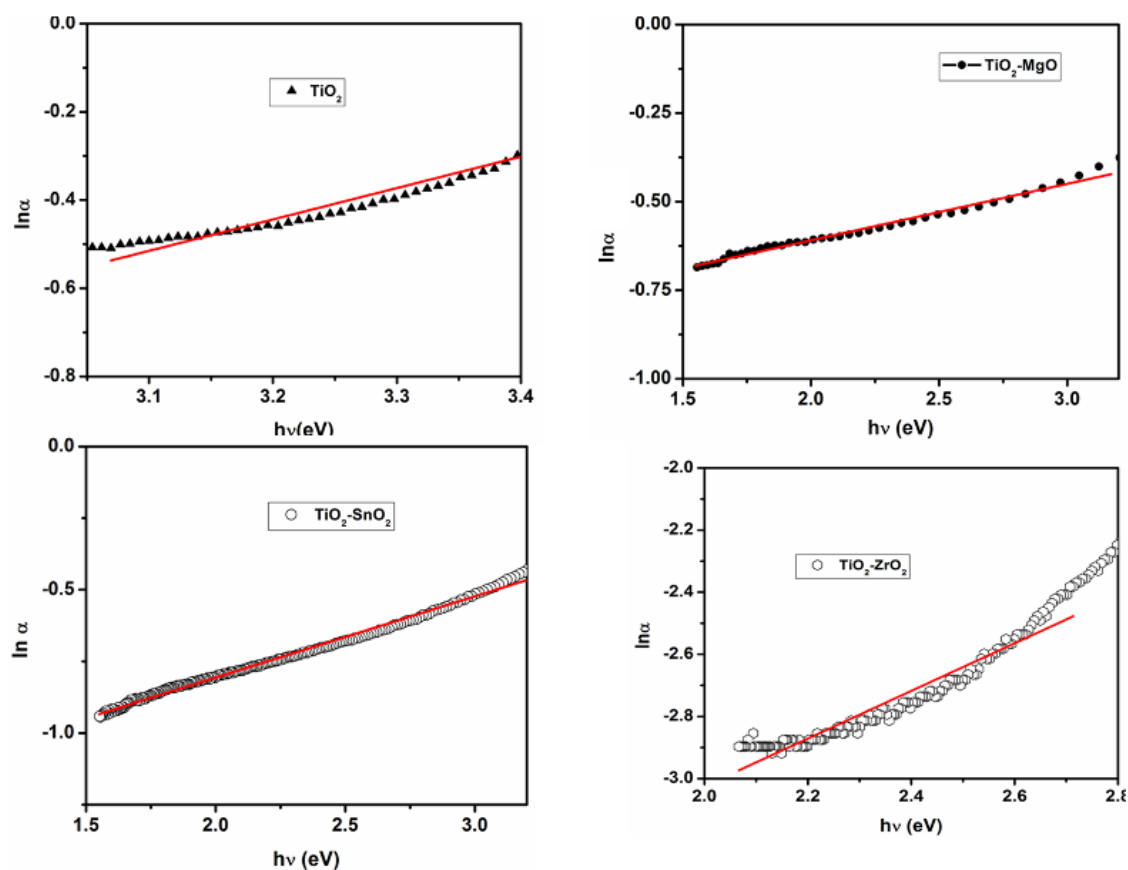
Fig. 6.4: Urbach tail plot of the core-shell structures

In case of bulk TiO_2, the Urbach tail is linked with the excitons self trapping, which is in agreement with the anatase phase as it has lower coordination among TiO_6 octahedra [3]. The Urbach energy is calculated by the equation as described in *chapter 3* (section 3.3.1 , page no.) and is presented in table 6.1.

Table 6.1: Calculation of band gap and Urbach energy

Sample name	Band gap (eV)	Urbach energy (meV)
TiO_2	3.4	1406
TiO_2-MgO	3.1	6289
TiO_2-SnO_2	3.2	3571
TiO_2-ZrO_2	2.7	1315

From the table we can see that there is tremendous increase in case of the core-shell films (TiO_2-MgO and TiO_2-SnO_2) than the core film. The growth of the shell leads to strain and the formation of defect states at the core/shell interface or within the shell.

These serve as trap states for photogenerated charge carriers. The excited electrons are captured by the shallow defect bands, preventing their direct transition to the conduction band as a result increasing the Urbach energy to such high extent. But in case of TiO_2-ZrO_2 film, there is a decrease in Urbach energy indicating less number of defect related traps in the film. A direct evidence of this is also prominent in the UV-vis absorbance spectra as there is no visible light related absorbance in the core-shell TiO_2-ZrO_2 film. From the band gap calculation it is significantly clear that all the core-shell films exhibit lower band gap than the core structure which directly hint towards the probability of TYPE 2 like core-shell formation.
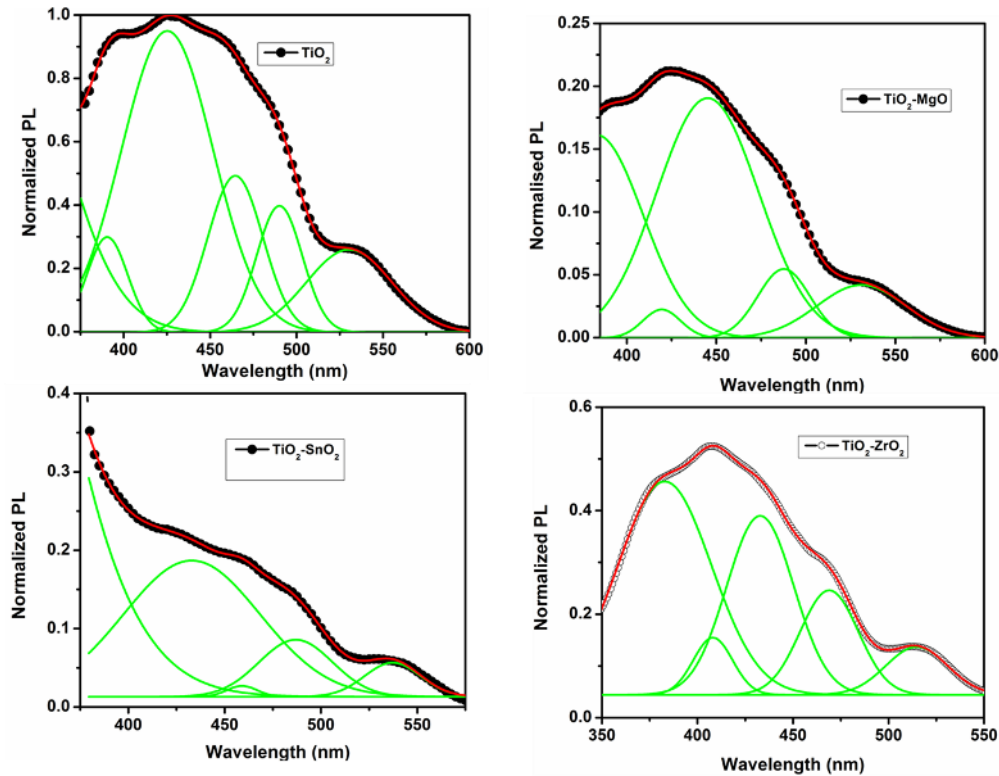
6.1.1.3 PL spectra analysis

Fig. 6.5: PL spectra of the prepared films

Fig. 6.5 displays the Gaussian fitted emission spectra of all the films excited at (330 nm). If we look at the PL spectrum of pure TiO_2 film we can see an emission peak at 390 nm. This peak is due to phonon assisted indirect transition from $M{\rightarrow}\Gamma$ in the Brillouin zone. The peak at ~425 nm is due to self trapped exciton emission. The other

peaks are attributed to oxygen vacancies and various defect related states present in the system. In case of core-shell TiO_2-MgO film, the 390 nm peak is not distinctly visible only a small hump is found around that region. The intensity of the hump is less than that of the band edge emission peak of TiO_2. Again, TiO_2-SnO_2 film exhibit no peak around that area only a tail to be found. This confirms the complete quenching of the peak due to very less charge recombination in the core-shell films. Thus the TYPE 2 structure is established in case of TiO_2-MgO and TiO_2-SnO_2 films.

But the TiO_2-ZrO_2 film tells a completely different story as the intensity of the 390 nm peak is further enhanced in the core-shell film. So, it does not comply with TYPE 2 structure. This may be due to lack of defect related states which enhanced charge recombination in the sample.

6.1.1.4 Electrical Characterization
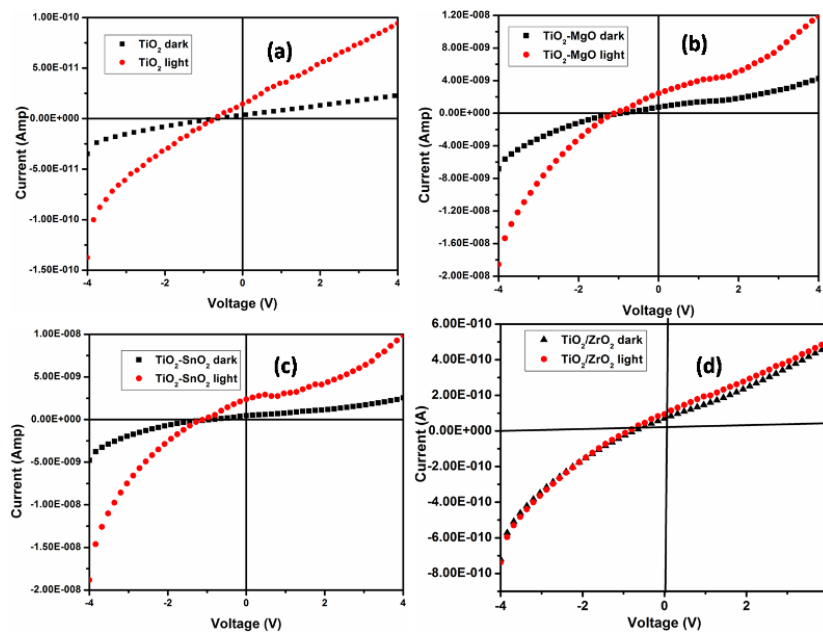
Fig. 6.6 : *I-V* Characteristic of (a) TiO_2 (b) TiO_2-MgO (c) TiO_2-SnO_2 and (d) TiO_2-ZrO_2 core-shell films

Fig. 6.6 shows the *I-V* characteristic of all the prepared films under dark as well as in illumination of a 6W visible light bulb. The electron transport mechanism in TiO_2 materials was studied by several researchers during the last decade [5-11]. It is well-

established that the electrical conductivity of a metal oxide in air is attributed to intrinsic defects and more precisely, to oxygen vacancies due to the stoichiometric deviation. Also, the physics of polycrystalline materials is based mostly on the grain boundary effect. According to this, a large number of defects surrounding boundaries strongly affect the carriers' charge driven process [11].

These defects serve as traps for the free charge carriers hereby reducing the electrical conduction. In our case, the small value of the dark conductivity can be caused by the lower density of the free charge carriers within the material, by the high barrier height at grain boundaries, or by a combination of both.

From the Fig 6.6, it is clearly visible that the magnitude of dark current is prominently lower in case of the illuminated films. Also while TiO_2 film showed photocurrent of 10^{-10} amp the core-shell TiO_2-SnO_2 and TiO_2-MgO films generated photocurrent of the order of 10^{-8} amp. When TiO_2 material is excited by the UV light having the photon energy equal to or greater than the TiO_2 band gap, electron-hole pairs are created and the electrons are promoted from the valence band to the conduction band leaving positive holes in the valence band. If the electrons and holes do not recombine they can undergo charge transfer processes such as reductive and oxidative reactions on the material surface [12-13]. But as we see while studying the photoelectrical behavior of the films under visible light illumination, it becomes very crucial for the TiO_2 nanoparticles embedded in the films to generate charge carriers as the energy of the light becomes lower than the band gap of the films. But still, some photocurrent are present due to two reasons. As we can all see from the UV-vis absorbance spectra, may it be little but some amount of visible absorbance is shown by the films which contribute to the photocurrent we obtained. Also as we have already explained in the earlier chapters TiO_2 and its corresponding core-shells are very ambient in charge separation which is found to the more prominent in the latter. That is why, as expected the photocurrent is increased by two fold in case of the core-shell films. But a jeopardy is seen in TiO_2-ZrO_2 film as it is unable to show any difference between dark current and photocurrent resulting in very less amount of photocurrent. This may be due to lack of defect related states which act as trap centers to separate the charge carriers for taking part in generating photocurrent.

The forward biased I-V characteristics of real p-n diodes are further affected by high injection and the series resistance of the diode [14]. As an example we have plotted the forward bias characteristic of TiO_2-MgO film (Fig. 6.7). They also resemble quite similarly to that of a *p-n* diode. We can divide the curve into four regimes. The region from 1.7 V to 2.9 V is ideal diode regime where the current increases linearly with increasing voltage. Theoretically this portion is considered to be having an ideality factor of 1. To the left of the ideal diode region, the current is subjugated by the trap-assisted recombination in the depletion region. This area is considered to have an ideality factor of 2. To the right of the ideal diode region, the current becomes restricted by high injection effects and by the series resistance.
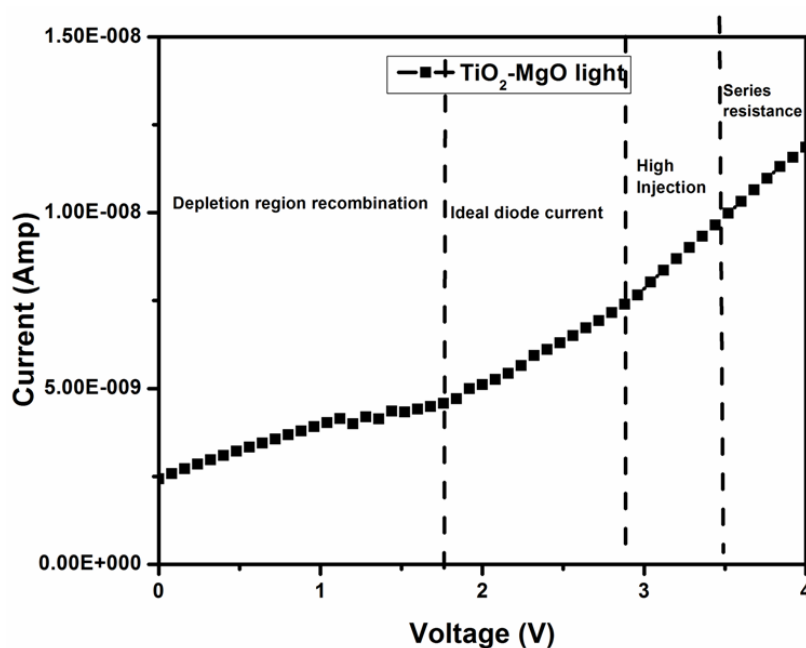

Fig. 6.7: Different characteristic regimes of the films

6.1.1.5 Photovoltaic characterization

Since from all characterizations performed to find out the materials which fulfill the essential conditions for a material to be used as photoanode, it is crystal clear that TiO_2-MgO and TiO_2-SnO_2 are making it up to a convenient extent; we tried to fabricate simple photovoltaic device with a cost effective laboratory method with these samples.

6.2   Photovoltaic device fabrication

Thus, we can see from the spectroscopic and electrical analysis of the core-shell films that TiO_2 film, core-shell TiO_2-SnO_2 film and TiO_2-MgO film are fulfilling the basic requirements to be used in a photovoltaic device. So, we fabricated the photoanodes as described in the following sections.

6.2.1 Photoanode fabrication

The films that we fabricated as described are dipped in a dye solution for 24 hours to obtain the photoanode. The dye solution is prepared using 20 ml of 1mM of Eosin Y in ethanol. Then after 1 day of complete immersion, the film is taken out and heated at $70^{°}C$ to get the desired photoanode.

6.2.2 Photocathode fabrication

The photocathode is an ITO glass where Pt deposited by sputtering method.

6.2.3   Electrolyte synthesis

A 0.5M lithium iodide and 0.05M iodine solution in acetonitrile was prepared and used as electrolyte [15].

6.2.4 Device fabrication

A spacer of parafilm was placed on the photoanode with several holes in it. Then few drops of electrolyte were added quickly and the photocathode is sandwiched upon the photoanode. These anode and cathode are bound tightly with the help of two binder clips. The light source used was a xenon lamp of 500 W and a Keithley 2400 sourcemeter was used to record datas for the *I-V* graph.

From the Fig. 6.8, it can be seen that the active area of the graph belongs to the forth quadrant of the *I-V* characteristic. The values of the parameters are obtained are presented in table 6.2.
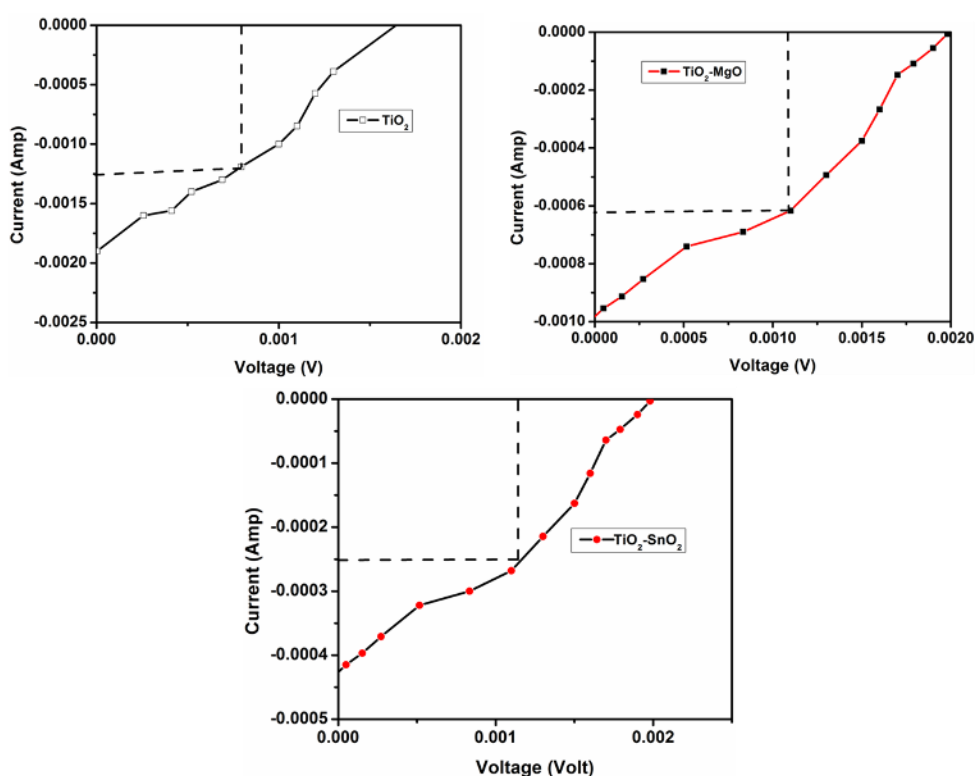
Fig. 6.8:   Photovoltaic characterization under visible light illumination

Table 6.2: Calculation of fill factor of the devices

Sample name	$V_{oc}(V)$	$I_{sc}(A)$	$V_m(V)$	$I_m(A)$	Fill factor (FF)
TiO_2	0.0016	-0.0019	0.00082	-0.001	0.23
TiO_2-MgO	0.0018	-0.000984	0.001	-0.000625	0.58
TiO_2-SnO_2	0.0019	-0.00042	0.0011	-0.000251	0.34

From the table 6.2, we can see that the open circuit voltage is increased in the core-shell films than that in the core film. Since the core-shell electrodes provide an inherent energy barrier at the electrode–electrolyte interface, the electron recombination losses are remarkably reduced and, consequently, the *Voc* values increase [1]. This energy barrier repressed back ransfer of TiO_2 electrons to electrolyte thereby reducing charge recombination. In case of TiO_2-MgO photoanode, where fill factor is obtained as maximum (0.58), this can be explained from the point of the isoelectric point (IEP) of MgO and TiO_2. IEP means pH at which an immersed oxide

surface has zero net charge. If pI (IEP) of an immersed oxide is lower than pH of the solution, the solid oxide surface has negative charge. If pI of an immersed oxide is higher than pH of the solution, the solid oxide surface has positive charge. The IEPs of TiO_2 and MgO are 6.2 and 12.4, respectively [16]. Thus, the MgO surface in an immersing solution (electrolyte in this case) is more positive than the TiO_2 surface due to the higher IEP of MgO. This indicates that the attractive force between MgO surface and dye molecules is stronger than that of TiO_2 surface and dye molecules. Thus the intermediate MgO layer prevents charge recombination between the TiO_2 layer and the electrolytes yielding a very good fill factor.

6.3   Conclusion

Thus in the chapter we attempted our best to deal with the questions those mentioned at the very beginning of the chapter. We found that most of the optical properties did not alter when the nanoparticles were caste on substrates whilst significant change was observed in TiO_2-ZrO_2 film.. Also we studied the electrical as well as photovoltaic properties with a very simple and cost effective method only to find that the core-shell films performed far better than the core film as a photoanode. So, there is future scope in working on these core-shell structures with proper sophisticated instruments to attain better fill factor.

References

[1] Avellaneda. C. O., et al. Preparation and characterization of core-shell electrodes for application in gel electrolyte-based dye-sensitized solar cells, *Electrochimica Acta* **55**, 1468--1474, 2010.

[2] Sekiya, T et al., Absorption spectra of anatase TiO2 single crystals heat treated under oxygen atmosphere, *J. Phys. Chem. Solid.* **61** (8), 1237--1242, 2000.

[3] Kuznetsov, V.N., & Krutitskaya, T.K. Nature of color centers in reduced titanium dioxide, *Kinet. Catal.* **37** (3), 446--449, 1996.

[4] Komaguchi, K., et al. Electron transfer reactions of oxygen species on TiO2 nanoparticles induced by sub band gap illumination, *J. Phys. Chem. C*. **114** (2), 1240--1245, 2010.

[65] Kuznetsov, V.N., & Serpone, N. On the origin of spectral bands in the visible spectral bands   in the visible absorption spectra light active TiO2 specimens analysis and assignments, *J. Phys. Chem. C.* **113** (34), 15110--15123, 2009.

[5] Yildiz, A., et al. Electrical properties of TiO_2 thin films, *J. Non-Cryst. Solids*. **354**, 4944--4947, 2008.

[6] Huber, B., et al. Nanocrystalline anatase TiO_2 thin films: preparation and crystallite size-dependent properties, *Thin Solid Films* **472**, 114--124, 2005.

[7] Yildiz, A., et al. The thickness effect on the electrical conduction mechanism in titanium oxide thin films, *J. Alloys. Compd.* **493**, 227--232, 2010.

[8] Villafuerte, M ., et al. Hysteretic current–voltage characteristics in RF-sputtered nanocrystalline TiO_2 thin films , *Physica B* **398**, 321--324, 2007.

[9] Mardare, D., et al. On the structure, morphology and electrical conductivities of titanium oxide thin films *Surf.Sci.* **507-510**, 468--472, 2002.

[10] Maurya, P. C., et al. Structural, optical and charge transport study of rutile TiO_2 nanocrystals at two calcination temperatures, *J. Alloys Compd.***509**, 8433--8440, 2011.

[11] Bartic M., et al. Optical and electrical properties of tio2thin films deposited by sol-gel method, *Rev. Roum. Chim.* **58 (2-3)**, 105--111, 2013.

[12] Linsebigler, A.L., et al. Photocatalysis on TiO_2 Surfaces: Principles, Mechanisms, and Selected Results, *Chem. Rev.* **95**, 735--758, 1995.

[13] Skubal, L.R., et al. Detection and identification of gaseous organics using a TiO_2 sensor , *J. Photochem. Photobiol.A* . **148**, 103--108, 2002.

[14] B. Van Zeghbroeck, Principles of Semiconductor Devices and Heterojunction, Prentice Hall PTR, 2007.

[15] Takechi, K., Muszynski,R., and Kamat,.V., Fabrication procedure of dye-sensitized solar cells, http://www3.nd.edu/~pkamat/pdf/solarcell.pdf.

 [16] Park. H., et al Fabrication of MgO-coated TiO$_2$ nanotubes and application to dye-sensitized solar cells, *J. Electroceram.* **23**, 146--149, 2009.